surfaces

MDPI

Article

UV Light Driven Selective Oxidation of Cyclohexane in Gaseous Phase Using Mo-Functionalized Zeolites

Vincenzo Vaiano * and Diana Sannino

Department of Industrial Engineering, University of Salerno, Via Giovanni Paolo II 132, 84084 Fisciano (Salerno), Italy; dsannino@unisa.it

* Correspondence: vvaiano@unisa.it; Tel.: +39089964006

Received: 31 October 2019; Accepted: 5 December 2019; Published: 9 December 2019



Abstract: Heterogeneous photocatalysis in the gas phase has been applied as a promising technique for organic syntheses in mild conditions. Modified zeolites have been used under UV irradiation as novel photocatalysts. In this study, we preliminarily investigated the photoxidation of cyclohexane on ferrierite and MoO_x-functionalized ferrierite in a gas–solid continuous flow reactor. In the presence of UV light, MoO_x-functionalized ferrierite showed the formation of benzene and cyclohexene as reaction products, indicating the occurrence of photocatalysed cyclohexane oxydehydrogenation. By contrast, unmodified ammonium ferrierite exhibited relevant activity for total oxidation of cyclohexane to carbon dioxide and water. The influence of Mo loading on cyclohexane conversion and products selectivity was evaluated.

Keywords: cyclohexane; photooxidation; benzene; cyclohexene; molybdenum oxides; ferrierite

1. Introduction

Direct oxidations of small hydrocarbons by O_2 are very unselective because of the free radical nature of the process, the high exotermicity of the reactions and/or overoxidation [1].

Heterogeneous photocatalysis has been deeply studied as a novel method for environmental detoxification both in water and in air. Some papers are devoted to the application of heterogeneous photocatalysis in organic synthesis at ambient temperature and pressure.

Titania is by far the most-widely applied photocatalyst since it is a stable, non-toxic, cheap semiconductor, but it presents some disadvantages, such as activation only through UV-A radiation, the low surface area that induces a limited adsorption of the chemical substances to be photoconverted, and a certain easiness of recombination in form of heat of photogenerated carriers.

Indeed, under UV irradiation with photons having an energy equal or higher to that of the band gap, the semiconductor generates electron–hole pairs that migrate on the surface of the photocatalyst. The holes may interact with adsorbed species on the surface, such as H_2O or OH^-, yielding highly reactive hydroxyl radicals, able to react with adsorbed species, while the e^- in the conduction band with the adsorbed O_2 gives superoxide, which in turn, can give redox reactions with the substances presents at the photocatalyst surface. As a consequence the photoxidation is ruled also by the adsorption of molecules on the photocatalyst surface. Competitive adsorption is often a key aspect in the photoconversion of different substances, or the presence of selective adsorption can improve the rate of photoconversion of a certain molecule [2].

Corma et al. [3] have reported the advantageous use of zeolites in photocatalysis.

Zeolites are crystalline inorganic materials, the largest family belonging to aluminosilicate. They possess a nanoporous structure, with a framework composed of interconnected channels or cavities nanometric or subnanometric in size, labelled as micropores (0.5–2 nm) [4]. This nanoporosity confers a high microporous internal volume accessible to reactants. The pores are uniform in size,

and moreover there is a polar environment, due to the substitution of Si(IV) with Al(III), which yields in a negative charge on the framework internally balanced by different cations. The zeolites have internal active sites and excellent adsorption ability, and exhibit molecular sieves effects with regard to different molecules. In photocatalysis zeolite offer (i) high porous volume (useful to get high adsorption of reactants to be photo-oxidised or reduced), (ii) high transparency to UV–radiation above 240 nm (permitting the activation of a photoactive guest, (iii) opportunity to change their chemical composition, by varying the atoms in the framework and/or in extra-framework positions, yielding in photoactive sites if photosensitive species are added, (iv) chance to tune the micropolarity of the zeolite internal porous volume and to select the size of the channels [5].

There are several research paper showing the selective adsorption of a chemical using the shape-selectivity of zeolites [6] or the so-called adsorb-and-shuttle concept [2,7]. These approaches in photocatalysis exploit the selective adsorption to improve or promote the mineralization. It has been demonstrated that it's possible to enhance the photocatalytic activity and selectivity yielding the zeolite framework photoactive or by entrapping semiconductor oxides inside the zeolite structure [8]. g the zeolite framework can be modified through the incorporation of heteroatoms (Ti and other transition metals), yielding the zeolite a material with photocatalytic properties [9,10]. However the photoactivity will depend from the degree of photoactive elements in the framework.

The semiconductor oxides can be incorporated into the zeolite cavities either by ion exchange or by hydrothermal method [11,12]. In this type of hybrid materials, the unique characteristics of zeolite structure can be exploited. The composites can be formed encapsulating the semiconductors and the crystal structure of the zeolite tunes the size of the semiconductor nanoparticles. The polar environment favours the photoinduced electron transfer and minimizes the electron-hole recombination rate [13].

The most representative semiconductor/zeolite photocatalyst is TiO_2 @ zeolite, which has been widely studied in recent years. It was found that TiO_2 @ zeolite is efficient for the decomposition of NO [14], for the efficient elimination of NH_3 and H_2S from air [15] and for CO_2 reduction [16]. TiO_2 @ zeolite is also efficient for the selective photoreduction of CO_2 to CH_3OH with minor concentration of CO and O_2 [17]. Some papers have demonstrated that TiO_2/zeolite composites showed an enhanced photo-degradation activity of phenol and chlorophenol [18], likely due to the higher adsorption properties of the zeolite and therefore facilitating the photodegradation activity of TiO_2.

An example of advancement by the use TiO_2/zeolite composite is reported in [19] where NH_4–Ag/ferrierite functionalized with TiO_2 was supported on ceramic tiles to increase the self-cleaning properties.

In the cation-exanchanged zeolite, the generation of radical cation O^{2-} pair can be achieved in mild condition, controlling the chemistry of radicals and primary oxidation products [20].

The selective photoxidation of liquid benzene by O_2 in CH_3CN/H_2O solution was studied with transition metal-exchanged BEA zeolites [21]. Another work reported cation-exchanged Y zeolite (such as NaY and BaY) showing photocatalytic activity for the partial oxidation of cyclohexane to cyclohexanone and cyclohexanol with molecular oxygen in a slurry reactor [22]. At the best of our knowledge, very few papers are devoted to the application of ferrierite zeolite to photocatalytic investigations for the chemical synthesis of value added organic compounds.

The ferrierite is found in nature with a SiO_2/Al_2O_3 ratio varying around an average value of 12. The framework structure consists of chains of five member rings (5-MRs) in the ab plane, connected through 10- and 6-MR elements, and forming vertically a two-dimensional network of 10-MR and 8-MR pores. The pores size are 0.43 × 0.55 and 0.34 × 0.48 nm for the 10-MR and 8-MR channels, respectively. The ferrierite could be also synthetic in origin and the structure type is indicated as FER. FER has an orthorombic symmetry with a = 1.92, b = 1.41, and c = 0.75 nm as unit-cell dimensions. The unit cell is composed by 36 tetrahedral atoms. A detailed structural study of a synthetic FER and exchanged forms is reported in [23].

The ferrierite adsorbs benzene, toluene and cyclohexane and performs as a medium port molecular sieve. The adsorption ability of ferrierite is enhanced by acid treatments, which implies no changing in the crystal structure [24]. For this reason the focus of the work was pointed on the application of ferrierite for the photocatalytic partial oxidation of cyclohexane in gas phase. It must be taken into account that most of the literature efforts are devoted to cyclohexane photoconversion in liquid phase.

With regard to gas phase selective photocatalytic oxidation reactions, the heterogeneous photocatalytic partial oxidation of cyclohexane was studied on Au/TiO_2 photocatalysts at different gold loadings in a gas-solid photocatalytic fluidized bed reactor at high illumination efficiency, observing, as main products, cyclohexanol, cyclohexanone, and CO_2 with a selectivity strongly influenced by the gold content [25].

Moreover it was also investigated the photoconversion of cyclohexane on MoO_x supported on grafted TiO_2/SiO_2, exploring different loading of sulphate and Mo. Photocatalytic tests showed that benzene was the main reaction product formed during irradiation with together CO_2 and cyclohexene as by products [26].

The photocatalytic oxidative dehydrogenation of cyclohexane on sulphated $MoO_x/\gamma\text{-}Al_2O_3$ catalysts [27] evidenced the effect of Mo loading at similar sulphate content and the effect of catalyst preparation method, achieving an almost total selectivity to cyclohexene. The catalyst selectivity is dependent on the modulation of surface acidity.

Unsulphated and sulphated titania are both active in cyclohexane total oxidation, but sulphate doping of titania induces a slowing in the reaction rate. On Mo-based catalysts, polymolybdate species enabled titania to transform cyclohexane to benzene and cyclohexene, reducing at zero the formation of CO_2 [28].

As pointed above, no paper reports the application of zeolites in gas-phase photocatalytic selective oxidation. Therefore, in this study, we preliminarily investigated the photoxidation of cyclohexane on ferrierite and MoO_x-ferrierite in a gas-solid continuous flow reactor.

2. Materials and Methods

2.1. Samples Preparation and Characterization

Zeolitic catalysts were prepared starting from Na, K–ferrierite ($K_{2.7}Na_{1.1}Si_{32.2}Al_{3.8}O_{72}$ $12H_2O$, Engelhard-ferrierite EZTM-500, Engelhard Corporation, Iselin, NJ, USA), with Si/Al ratio of 8.4. The characteristics of the Na, K-ferrierite are shown in Table 1.

Table 1. Characteristics of Na, K-Ferrierite.

Bulk Density, g/cm^3	0.40
Pores Diameter, Å	4.0
SiO_2, Dry wt %	84.9
Al_2O_3, Dry wt %	8.6
Na_2O, Dry wt %	1.5
K_2O, Dry wt %	5.6
K_2O/Al_2O_3	0.7
Na_2O/Al_2O_3	0.28
SiO_2/Al_2O_3	16.8

Ferrierite was ion exchanged to ammonium form with 1 M solution of ammonium nitrate in order to obtain the NH_4 form (AFer). Powdered catalysts were prepared by wet impregnation of Afer with an aqueous solution of ammonium heptamolybdate $(NH_4)_6$ $Mo_7O_{24}{\cdot}4H_2O$, drying at 120 °C for 12 h and calcination in air at 550 °C for 3 h. Table 2 contains the list of samples prepared with indications of the nominal MoO_3 load.

Table 2. List of catalysts with their MoO_3 nominal content.

Catalyst	Nominal MoO_3 Content (wt %)
AFer	-
5MoAFer	5.0
20MoAFer	20.0

The prepared photocatalysts were analyzed with different chemical-physical characterization techniques. The analysis of molybdenum amount in the photocatalysts was affected by inductively coupled plasma mass spectroscopy (ICP-MS 7500 Agilent spectrophotometer, Agilent Technologies Inc., Santa Clara, CA, USA)). Before the analysis, the samples were mineralized by microwaves apparatus with a mixture of hydrofluoric and hydrochloric acid, dried at high temperature, then dissolved with ultra-pure nitric acid in Millipore Q water [29]. Thermogravimetric analysis (TGA) was performed in air (at a heating rate of 20 °C min^{-1}) using SDTQ600 (TA Instruments, New Castle, DE, USA) thermal analyser. In order to study the porosity of catalysts powder, the adsorption-desorption isotherms of the samples were determined by N_2 adsorption-desorption at −196 °C with a Thermoquest Sorptomatic 1990 (Thermoquest, Waltham, MA, USA). In this case, powder samples were outgassed (10^{-4} Torr) and heated to 450 °C before each test. Fourier Transform Infrared (FTIR) spectroscopy was performed in the 4000–400 cm^{-1} range with a resolution of 2 cm^{-1}. To acquire the spectra, a Bruker IFS 66 FTIR spectrophotometer (Bruker Italy, Milano, Italy) was used. Samples were diluted at 1 wt % in KBr. The mixture was ground and a transparent disk of 100 mg was prepared with a press in vacuum. Disks are introduced into the proper chamber of the instruments and the scan was carried out at room temperature. UV–vis reflectance spectra of powder catalysts were acquired by a Perkin-Elmer spectrophotometer Lambda 35 (PerkinElmer Italia, Milano, Italy), equipped with RSA-PE-20 reflectance sphere (Labsphere Inc., North Sutton, NH, USA). The sample holder was inclined of 8° and the reflectance was related to a calibrated standard SRS-010-99 (Labsphere Inc., North Sutton, NH, USA). The reflectance data were reported as Kubelka–Munk values versus the wavelength. Equivalent band gap determinations were computed, assuming that the dispersed MoO_x phase behaves as direct gap semiconductor. The plot of $[F(R\infty) \times h\nu]^2$ as a function of $h\nu$ (eV) permits the evaluation of the intercept of a line passing through $0.5 < F(R\infty) < 0.8$.

2.2. Photocatalytic Activity Tests

Photocatalytic activity tests were performed using the laboratory apparatus shown in Figure 1. It consists of three sections:

- Feed section;
- Reaction section; and
- Gas composition analysis section.

All the gas pipes ($\frac{1}{4}$" external diameter) are of Teflon, connections are made with Swagelok union and two, three and four way Nupro valves. All the connections are in stainless steel to avoid any corrosion due to the presence of water. All the gases come from SOL SPA with a purity degree of 99.999%.

Oxygen and nitrogen were fed from cylinders, nitrogen being the carrier gas for cyclohexane (CH) and water vaporized from two temperature controlled saturators. To feed an accurately controlled flow, Brooks measured flow controllers (MFC) are used, able to operate with a maximum pressure drop of 3 atm. A rotameter for N_2 is used for vaporizing water to feed to the reactor. In the reaction section a system of valves allows the reactants to go to the reactor, and the products to the analysis section, or, in the bypass position, the reactants to the analysis section to verify the reactant composition.

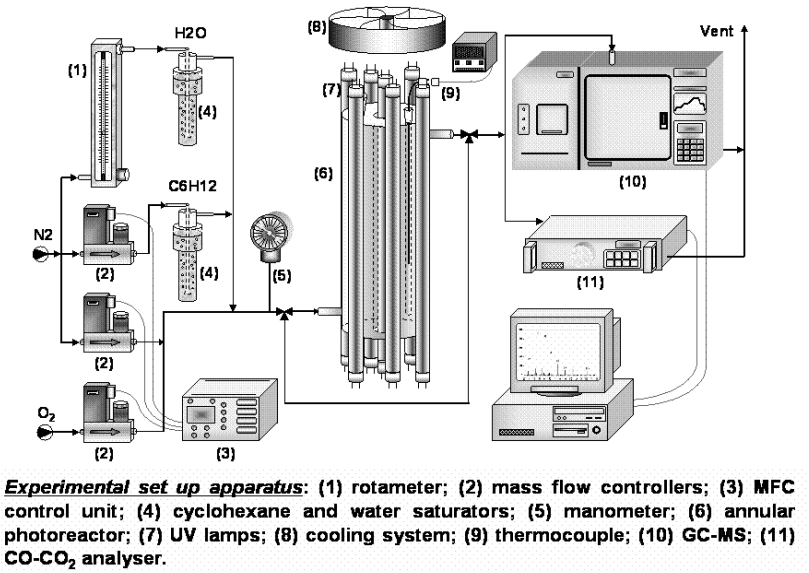


Figure 1. Laboratory apparatus for photocatalytic activity tests [30].

A fixed bed photocatalytic reactor (reactor volume: 7 L) with an anular section was used. The reactor is composed by two co-axially mounted 500 mm long quartz tubes having 140 and 40 mm diameter, respectively. The reactor was irradiated by seven 40 W UV fluorescent lamps emitting photons at wavelengths in the range 300–425 nm, centred at 365 nm. One lamp (UVA Cleo Performance 40 W, Philips, Milan, Italy) was positioned inside the inner tube and the remaining lamps (R-UVA TLK 40 W/10R flood lamp, Philips, Milan, Italy) were placed symmetrically around the external transparent surface of the reactor. The overall photocatalytic system was surrounded with reflectant aluminum foils. The temperature was controlled to 35 ± 2 °C by cooling fans. The fixed bed of the catalytic reactor was composed by quartz flakes coated in situ with aqueous slurry of catalysts powder. The coated flakes were dried at 20 °C for 24 h. A uniform coating, well adhering to the quartz flakes surface, was achieved. The amount of deposited catalyst, evaluated by weighing the reactor before and after the coating treatment was 20 g. CO and CO_2 concentration at the outlet of the reactor was measured by an on line non dispersive IR analyser (Uras 10, Hartmann and Braun, ABB, Milan, Italy). Cyclohexane and reaction products were analysed by an on line quadrupole mass detector (MD800, ThermoFinnigan, Silicon valley, CA, USA). Catalytic tests were carried out feeding 830 Ncc/min N_2 stream containing 1000 ppm cyclohexane, 1500 ppm oxygen and adding 1600 ppm water. The latter substance was fed to minimise possible catalyst photodeactivation phenomena [31].

The catalytic performance was evaluated as:

CH% conversion = 100 × (moles of inlet CH – moles of outlet CH)/(moles of inlet CH)
BE% selectivity = 100 × (moles of outlet BE)/(moles of inlet CH – moles of outlet CH)
CO_2% selectivity = 100 × (moles of outlet CO_2)/6 × (moles of inlet CH – moles of outlet CH)

where CH is for cyclohexane and BE for benzene.

3. Results and Discussion

3.1. Physical-Chemical Characterization Results

Thermogravimetric analyses were carried out on zeolites used as support. Figure 2 shows the thermogravimetric (TG) and first derivative (DTG) curves of ferrierite in ammonium form (AFer) and of hydrogen ferrierite (HFer) obtained after calcination of AFer at 550 °C in air for 2 h.

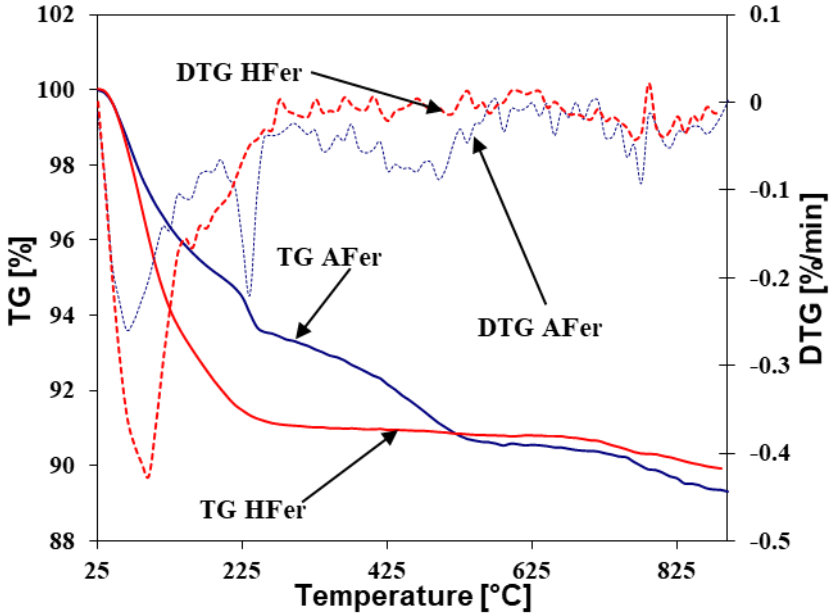


Figure 2. Thermogravimetric analysis of AFer and HFer.

As evidenced by the DTG minima, the two samples showed an initial weight loss at temperatures lower than 120 °C due to the adsorbed water loss. AFer sample showed a second weight loss in the 200–500 °C range, which is absent in HFeR, due to ammonium decomposition. In both samples, another weight loss is present around 800 °C, due to water formed by hydroxyl condensation with the consequent collapse of the zeolite structure.

The porosity characteristics were obtained by N_2 adsorption-desorption at −196 °C. The obtained results are reported in Figure 3.

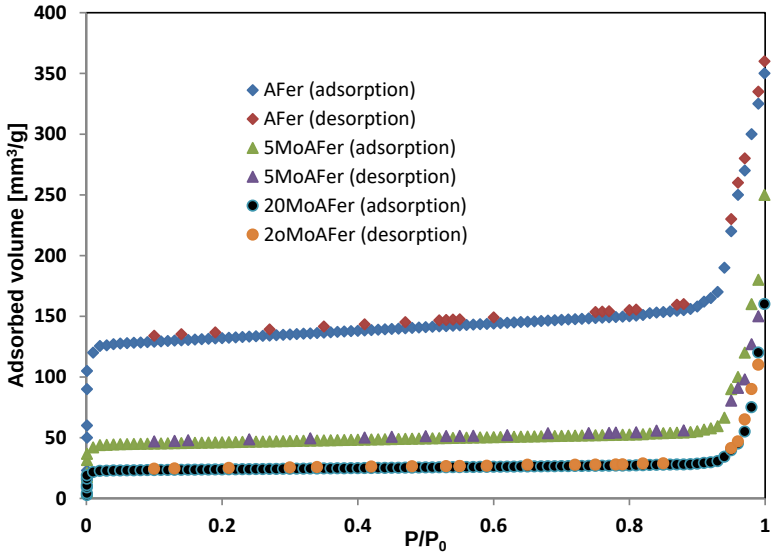


Figure 3. N_2 adsorption-desorption isotherms at −196 °C for AFer 5MoAFer and 20MoAFer samples.

The experimental data evidenced the microporous structure of parent AFer sample. Moreover, all the analysed photocatalysts showed very similar isotherms close to a type I, characteristic of microporous solids according to the IUPAC classification [32]. At higher relative pressures, the isotherms of MoFer solids show a very small hysteresis loop, evidencing low interparticles porosity.

The microporous volume was obtained by the Dubinin method and its value for all the samples are shown in Table 3.

Table 3. Microporous volume of zeolite-based samples and measured MoO_3 content.

Catalyst	Microporous Volume (cm^3/g)	Measured MoO_3 Content (wt %)	Equivalent Band Gap Energy (eV)
AFer	0.130	-	-
5MoAFer	0.045	4.7	3.2
20MoAFer	0.024	18.5	3.3

The results obtained evidenced that the addition of molybdenum on zeolite structure, leads to a microporous volume reduction and in particular for MoO_x/AFer samples, the microporous volume decreases with increase in Mo-loading. The strong reduction of microporous volume suggests the occlusion of zeolites pores by the molybdate species. Moreover, it can be seen that MoO_3 loadings evaluated by ICP-MS analysis are approximately equal to that one calculated for the impregnation process.

UV–VIS DRS spectra (not reported) were elaborated in order to determine the equivalent band gap energy for 5MoAFer and 20 MoAFer photocatalysts. The values are reported in Table 3.

The band gap energy was similar to that of MoO_3 (3.2 eV) [27] and indicates that both photocatalysts can be activated only by UV light.

FTIR spectra of AFer, 5MoAFer and 20MoAFer are contained in Figure 4. On all the samples, typical absorption bands of ferrierite in the range 400–1200 cm^{-1} are visible [33,34]. Absorption at 1072 cm^{-1} is assigned to asymmetric stretching of SiO_4 and AlO_4^- tetrahedrons, while at 802 cm^{-1} to symmetric vibration. Bands at 594 and 533 cm^{-1} are related to double ring vibrations. Pore opening bands are at 461 and 437cm^{-1} are also detectable.

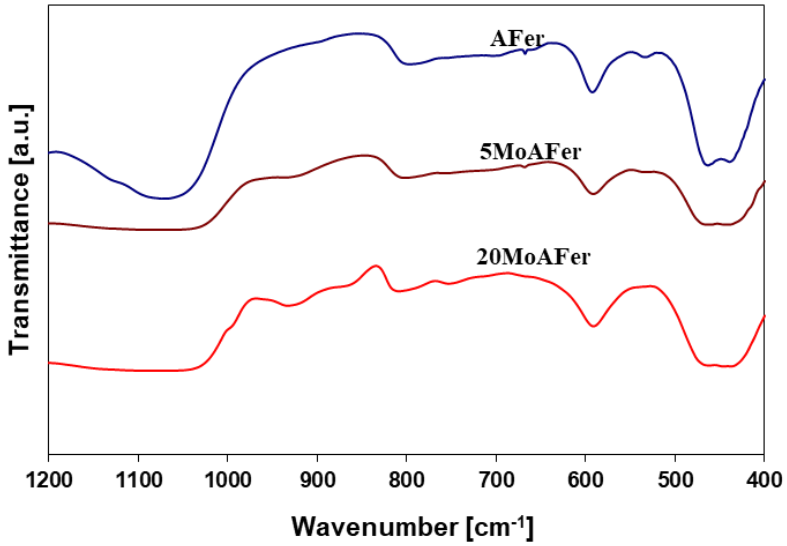


Figure 4. FTIR spectra of AFer 5MoAFer and 20MoAFer in the range 1200–400 cm^{-1}.

A more accurately analysis about the MoOx species can be obtained from the analysis of FTIR spectra in the range 1100–800 cm^{-1} (Figure 5).

Both 5MoAFer and 20MoAFer show a characteristic band at around 920 cm^{-1} usually attributed to Mo=O vibration of tetrahedral species MoO_4^{2-} [35] and the intensity of this band increases with Mo content. It is reported that FTIR spectra of Mo–V/HZSM5 catalysts present a shoulder band in the range 890–910 cm^{-1}, similar to Mo exchanged with Na–Y zeolite, corresponding to the Mo–O bond vibration in monomeric MoO_4^{2-}. However this shoulder band can be attributed also to the Mo–O–Al or Mo–O–Si vibrations or to the bending of the Mo–O bonds in $Al_2(MoO_4)_3$ [36]. As a consequence, the band at 920 cm^{-1} could indicate the presence of MoO_4^{2-} exchanged inside the ferrierite structure. On the

20MoAFer catalyst additional bands at 963 cm^{-1}, at 995 cm^{-1} and around 868 cm^{-1} (characteristics of MoO_3 crystallites) can be also observed [37].

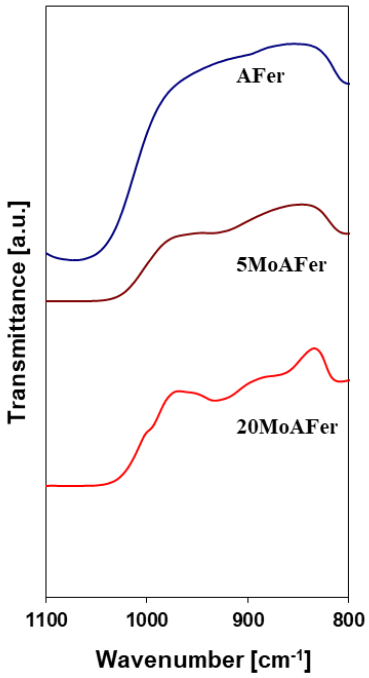


Figure 5. FTIR spectra of AFer, 5MoAFer and 20MoAFer in the range 1100–800 cm^{-1}.

The obtained results are consistent with the available literature. More in detail, the bands near 960 cm^{-1} can be assigned to the stretching mode of molybdenyl species in hydrated form [38,39]. In particular, they have been ascribed to terminal Mo=O stretching of octahedral polymeric surface species [38]. These results indicate that the formation of octahedral polymeric molybdate ($Mo_7O_{24}^{6-}$) is achieved for the 20MoAFer photocatalyst. Ng and Gulari [40] have reported from IR and Raman experiments that tetrahedral surface molybdates are detected at low loading, whereas at monolayer coverage, octahedrally-coordinated polymeric surface species are formed and, bulk molybdenum trioxide appears at high loading. Quincy et al. [41] reported similar results. Considering all the previous observations, it is possible to argue that, for the 5MoAFer sample, MoO_x are mainly present as tetrahedral species MoO_4^{2-}, probably linked to framework oxygens, whereas 20MoAFer displays the simultaneous presence of tetrahedral, octahedral polymeric molybdate and MoO_3 crystallites.

3.2. Photocatalytic Activity Results

Cyclohexane and CO_2 concentrations as functions of run time during a photocatalytic test on AFer are reported in Figure 6.

In the absence of irradiation, adsorption of cyclohexane was observed. When the lamps were light on, the cyclohexane concentration started to decrease up to 20% with respect to the inlet value and then progressively increased in the time, reaching a steady state value of about 15% of cyclohexane conversion after about 120 min. Simultaneously, CO_2 production of 220 ppm and no CO nor other oxidation products were detected. Thus, photocatalytic oxidation of cyclohexane on AFer leads to a complete mineralization into CO_2 and H_2O without formation of by-products.

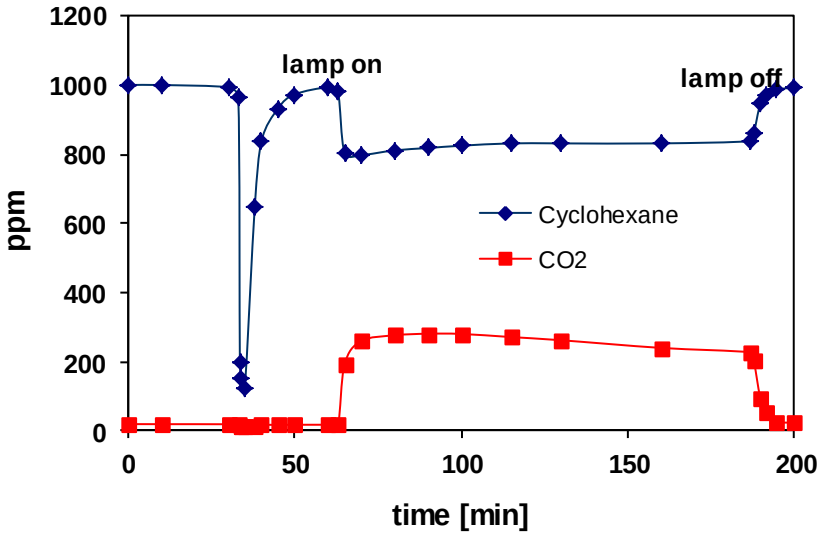


Figure 6. Outlet reactor concentration of cyclohexane and carbon dioxide as a function of run time on the AFer sample.

Reaction of photoxidation takes place within the ferrierite and can be considered to occur within an enclosed space, namely the 'reaction cavity'. The excited state of reactant molecules and their intermediates are confined in the reaction cavity during their lifetimes, so their mobility and flexibility will be limited or forced. The volume available for an organic molecule within cage and channels depends on the nature of exchanged cation. In the case of AFer the cation is NH_4^+ and a high microporous volume is observed. In general the zeolites offer a reaction cavity with "hard walls" and it is "active" because the interactions (weak van der Waals forces, hydrogen bonds, strong electrostatic forces between charged centres) between the guest molecule and the cavity are attractive or repulsive. The photochemical process is determined by both the guest and the host zeolite and the nature of chemical-physical interactions between them [20].

The catalytic properties of faujasite catalysts in oxidation of cyclohexane in gas phase were reported in [42]. Spectral studies have showed a strong adsorption of cyclohexane on NaY zeolite at low temperature and the comparison of characteristic absorption bands at 1720, 1780, and 1820 cm^{-1} attributed to carbonyl and peroxide compounds. It has been proposed that their formation occurs by the reaction of cyclohexane with the free radical forms of adsorbed oxygen and that further oxidation happens from the oxygen from the gas phase. As a consequence deep and oxidative dehydrogenation occur, giving rise to carbon dioxide and benzene [43].

In the case of photoactivity of AFer it is possible that thermal activation is substituted by UV–A photons activation. Indeed the very high electrostatic field in the zeolite cage can cause a red-shift of the cyclohexane O_2 charge-transfer transition, as verified trough the green or blue light irradiation of a cyclohexane and O_2 on NaY, resulting in the formation of cyclohexyl hydroperoxide and cyclohexanone with visible light [44]. These compounds can be considered as intermediates in the total oxidation of cyclohexane that instead occurs by far with AFer.

Different results were achieved in the photoxidation of cyclohexane on 5MoAFer and 20MoAFer (Figure 7). In these cases, the steady state cyclohexane conversion reached lower values (less than 1%), but the analysis of the reaction products disclosed the presence of benzene and cyclohexene, as identified from their characteristic mass fragments with together carbon dioxide. These results demonstrate that photocatalysed cyclohexane oxy-dehydrogenation to cyclohexene and benzene occurs on molybdenum-supported ferrierite since AFer alone exhibits high activity only in total oxidation to carbon dioxide but is not active for conversion to benzene and cyclohexene. Similar results were observed in the literature concerning the use of MoO_x-based photocatalysts in the gas phase cyclohexane selective oxidation [27,30,45,46].

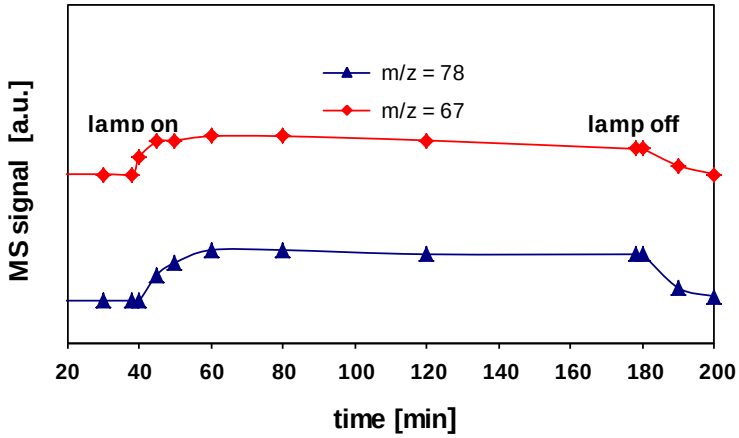


Figure 7. Behaviour of characteristics mass fragments at the outlet reactor of benzene (m/z = 78) and cyclohexene (m/z = 67) on 5MoAFer as a function of run time.

The influence of Mo loading on AFer was evaluated and obtained results are summarized in Figures 8–10.

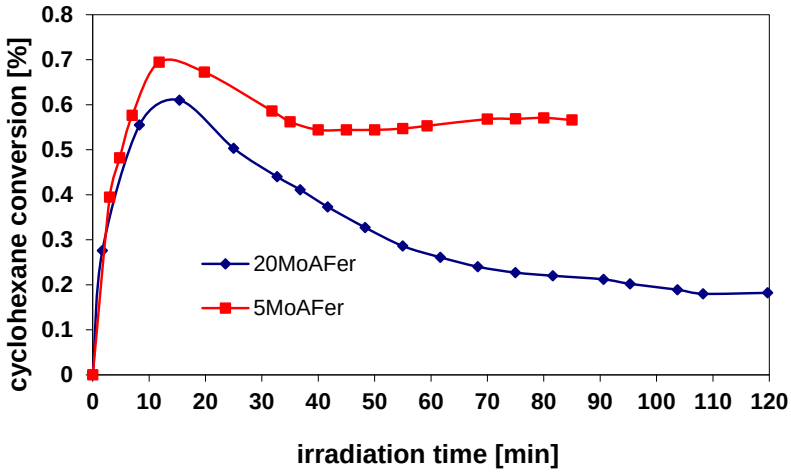


Figure 8. Cyclohexane conversion on 5MoAFer and 20MoAFer as a function of irradiation time.

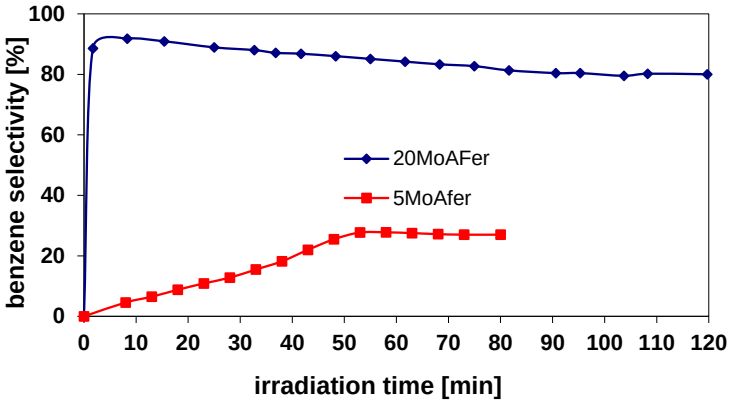


Figure 9. Benzene selectivity on 5MoAFer and 20MoAFer as a function of irradiation time.

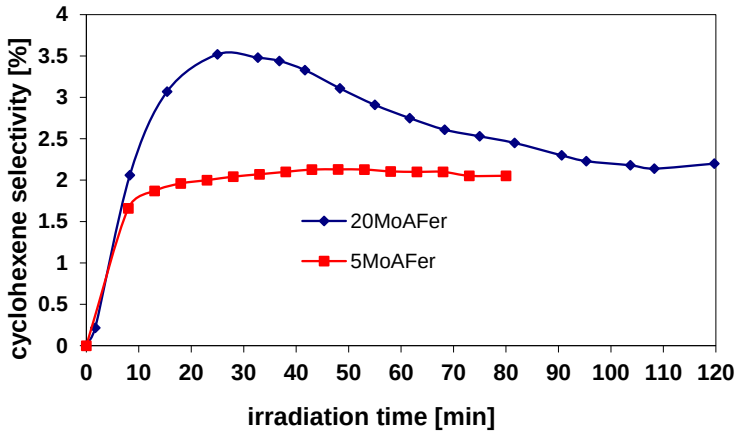


Figure 10. Cyclohexene selectivity on 5MoAFer and 20MoAFer as a function of irradiation time.

On both catalysts, after an irradiation time of 80 min, cyclohexane conversion obtained was less than 1% (about 0.6% on 5MoAFer and 0.2% on 20MoAFer). It reached a maximum value after about 15 min and then decreased to a steady state value, evidencing an initial catalyst deactivation. The lowest value of cyclohexane conversion on 20MoAFer could be explained considering the formation of MoO_3 crystallites on the zeolite, in agreement with literature findings about the photoxidative dehydrogenation of cyclohexane in gas phase [46].

Selectivity to benzene reached a very great steady state value (about 80%) on 20MoAFer while this value was 27% on 5MoAFer. On 20MoAFer benzene selectivity showed a value higher than 90% after about 10 min and then progressively decreased with irradiation time. Instead, on 5MoAFer, there was a progressive increase up to a steady state value. Similar behaviours were obtained for cyclohexene selectivity and its steady state value was very low for both catalysts (about 2% on 5MoAFer and 2.5% for 20MoAFer). In summary, there was a decrease of cyclohexane conversion and an increase of benzene and cyclohexene selectivity by increasing the Mo loading. It is interesting to note that with the increase of Mo loading, CO_2 selectivity was strongly reduced, taking into account the high value found on 5MoAFer (71%). The presence of polymolybdate anions enhances the oxidative dehydrogenation reactions, since the selectivity to CO_2 was further decreased to about 18% for 20MoAFer.

In summary, photocatalytic activity tests on all the catalysts evidenced that the presence of MoO_x species probably on the surface of AFer changes the selectivity of the catalyst with increasing molybdenum content indicating that the interaction between the zeolite and the molybdenum oxide species plays an essential role in changing the catalyst selectivity.

FTIR spectroscopy data coupled with photocatalytic activity results showed that the selective formation of benzene is likely due to the presence of polymolybdate species present on the AFer surface. It could be argued that polymolybdate species occupy the reaction cavities where the total oxidation of cyclohexane occurs. These results are consistent with our previous research studies dealing with MoO_x/TiO_2 and MoO_x/Al_2O_3 photocatalysts [27,46,47]. In these papers, it was also extensively reported that the photoexcited octahedral polymolybdate species are able to activate the photo-conversion of adsorbed cyclohexene to form benzene through hydrogen abstraction in liquid phase. It was also reported that photoexcited decatungstate is able to initiate the selective oxidation of the cyclohexane to cyclohexanol and cyclohexanone by means of a hydrogen abstraction mechanism in aqueous solution, followed by reoxidation of the tungstate by O_2 [48].

From these considerations, it is possible to hypothesize a possible mechanism of reaction involving the polymolybdate species in the selective conversion of cyclohexane to benzene and cyclohexene. In detail, the photoexcited octahedral molybdate (Equation (1)) is able to initiate the oxidative oxidative dehydrogenation of adsorbed cyclohexane to cyclohexene (Equation (2)), which may desorb

(Equation (3)) or in turn further oxy-dehydrogenate to benzene (Equation (4)) according to the following reactions [46]:

$$Mo_7O_{24}^{6-}/AFer + h\nu \rightarrow {}^*Mo_7O_{24}^{6-}/AFer \quad (1)$$

$$C_6H_{12}\ (ads) + 2{}^*Mo_7O_{24}^{6-}/AFer \rightarrow C_6H_{10}\ (ads) + 2HMo_7O_{24}^{6-}/AFer \quad (2)$$

$$C_6H_{10}\ (ads) \rightarrow C_6H_{10}\ (g) \quad (3)$$

$$C_6H_{10}\ (ads) + 4{}^*Mo_7O_{24}^{6-}/AFer \rightarrow C_6H_6(ads) + 4HMo_7O_{24}^{6-}/AFer \quad (4)$$

$$C_6H_6\ (ads) \rightarrow C_6H_6\ (g) \quad (5)$$

Photoreduced molybdate is than probably regenerated by the reactive oxygen species generated by the irradiation of the zeolite [20].

4. Conclusions

The occurrence of photocatalysed heterogeneous oxidative dehydrogenation of cyclohexane to benzene and cyclohexene in mild conditions has been preliminarily studied in a gas–solid annular photocatalytic fixed bed reactor in the presence of MoOx functionalized ferrierite, showing interesting selectivity to benzene and cyclohexene. The formation of polymolybdate species on the zeolite was observed on the MoO_x functionalized ferrierite, occluding the microporous volume of the AFer. This effect was beneficial in reducing the amount of carbon dioxide produced by the complete oxidation of cyclohexane, occurring in the absence of MoO_x species. Indeed, a very high selectivity to benzene (about 80%) was obtained at the highest investigated Mo loading (20 wt %). A preliminary mechanism for the photocatalytic action of polymolybdate was presented, evidencing the key role of these species towards the selective conversion of the cyclohexane to benzene and cyclohexene. However further studies are necessary to improve the low conversion of cyclohexane found on MoO_x functionalized ferrierite.

Author Contributions: Investigation: V.V.; writing—original draft preparation: V.V. and D.S.; writing—review and editing: D.S.

Funding: This research received no external funding.

Conflicts of Interest: The authors declare no conflict of interest.

References

1. Giannotti, C.; Richter, C. Photocatalysed oxidation of cyclohexane by $W_{10}O_{32}^{4-}$ irradiation with natural sunlight. *Int. J. Photoenergy* **1999**, *1*, 69–73. [CrossRef]
2. Paz, Y. Preferential photodegradation—Why and how? *Comptes Rendus Chim.* **2006**, *9*, 774–787. [CrossRef]
3. Corma, A.; Garcia, H. Zeolite-Based photocatalysts. *Chem. Commun.* **2004**, 1443–1459. [CrossRef] [PubMed]
4. Xu, R.; Pang, W.; Yu, J.; Huo, Q.; Chen, J. *Chemistry of Zeolites and Related Porous Materials: Synthesis and Structure*; John Wiley & Sons: Hoboken, NJ, USA, 2009.
5. Aramendía, M.; Colmenares, J.; López-Fernández, S.; Marinas, A.; Marinas, J.; Urbano, F. Screening of different zeolite-based catalysts for gas-phase selective photooxidation of propan-2-ol. *Catal. Today* **2007**, *129*, 102–109. [CrossRef]
6. Calza, P.; Pazé, C.; Pelizzetti, E.; Zecchina, A. Shape-Selective photocatalytic transformation of phenols in an aqueous medium. *Chem. Commun.* **2001**, 2130–2131. [CrossRef]
7. Sagatelian, Y.; Sharabi, D.; Paz, Y. Enhanced photodegradation of diisopropyl methyl phosphonate by the "adsorb & shuttle" approach. *J. Photochem. Photobiol. A Chem.* **2005**, *174*, 253–260.
8. Guo, Y.; Zu, B.; Dou, X. Zeolite-Based photocatalysts: A promising strategy for efficient photocatalysis. *J. Thermodyn. Catal.* **2013**, *4*, 1. [CrossRef]

9. Hashimoto, S. Zeolite photochemistry: Impact of zeolites on photochemistry and feedback from photochemistry to zeolite science. *J. Photochem. Photobiol. C Photochem. Rev.* **2003**, *4*, 19–49. [CrossRef]
10. Juan, Z.; Dishun, Z.; Liyan, Y.; Yongbo, L. Photocatalytic oxidation dibenzothiophene using TS-1. *Chem. Eng. J.* **2010**, *156*, 528–531. [CrossRef]
11. Liu, Z.; Liu, Z.; Wang, Y.; Li, Y.; Qu, L.; E, L.; Ya, J.; Huang, P. Photocatalysis of TiO_2 nanoparticles supported on natural zeolite. *Mater. Technol.* **2012**, *27*, 267–271. [CrossRef]
12. White, J.C.; Dutta, P.K. Assembly of nanoparticles in zeolite Y for the photocatalytic generation of hydrogen from water. *J. Phys. Chem. C* **2011**, *115*, 2938–2947. [CrossRef]
13. Bossmann, S.H.; Turro, C.; Schnabel, C.; Pokhrel, M.R.; Payawan, L.M.; Baumeister, B.; Wörner, M. $Ru(bpy)_3^{2+}/TiO_2$-codoped zeolites: Synthesis, characterization, and the role of TiO_2 in electron transfer photocatalysis. *J. Phys. Chem. B* **2001**, *105*, 5374–5382. [CrossRef]
14. Yamashita, H.; Ichihashi, Y.; Anpo, M.; Hashimoto, M.; Louis, C.; Che, M. Photocatalytic decomposition of NO at 275 K on titanium oxides included within Y-zeolite cavities: The structure and role of the active sites. *J. Phys. Chem.* **1996**, *100*, 16041–16044. [CrossRef]
15. Rasmussen, S.B.; Portela, R.; Suárez, S.; Coronado, J.M.; Rojas-Cervantes, M.L.; Avila, P.; Sánchez, B. Hybrid TiO_2—$SiMgO_x$ composite for combined chemisorption and photocatalytic elimination of gaseous H_2S. *Ind. Eng. Chem. Res.* **2010**, *49*, 6685–6690. [CrossRef]
16. Wang, C.; Thompson, R.L.; Baltrus, J.; Matranga, C. Visible light photoreduction of CO_2 using CdSe/Pt/TiO_2 heterostructured catalysts. *J. Phys. Chem. Lett.* **2009**, *1*, 48–53. [CrossRef]
17. Ikeue, K.; Yamashita, H.; Anpo, M. Photocatalytic reduction of CO_2 with H_2O on titanium oxides prepared within the FSM-16 mesoporous zeolite. *Chem. Lett.* **1999**, *28*, 1135–1136. [CrossRef]
18. Durgakumari, V.; Subrahmanyam, M.; Rao, K.S.; Ratnamala, A.; Noorjahan, M.; Tanaka, K. An easy and efficient use of TiO_2 supported HZSM-5 and TiO_2^+ HZSM-5 zeolite combinate in the photodegradation of aqueous phenol and p-chlorophenol. *Appl. Catal. A Gen.* **2002**, *234*, 155–165. [CrossRef]
19. Sarno, G.; Vaiano, V.; Sannino, D.; Ciambelli, P. Photocatalytic applications with TiO_2-zeolites composites anchored on ceramic tiles. *Chem. Eng.* **2015**, *43*. [CrossRef]
20. Ramamurthy, V. Controlling photochemical reactions via confinement: Zeolites. *J. Photochem. Photobiol. C Photochem. Rev.* **2000**, *1*, 145–166. [CrossRef]
21. Shimizu, K.-i.; Akahane, H.; Kodama, T.; Kitayama, Y. Selective photo-oxidation of benzene over transition metal-exchanged BEA zeolite. *Appl. Catal. A Gen.* **2004**, *269*, 75–80. [CrossRef]
22. Blatter, F.; Sun, H.; Vasenkov, S.; Frei, H. Photocatalyzed oxidation in zeolite cages. *Catal. Today* **1998**, *41*, 297–309. [CrossRef]
23. Ciambelli, P.; Sannino, D.; Palo, E.; Gargano, G.; Balboni, E.; Martucci, A.; Dalconi, M.; Alberti, A. Relevance of Co, Ag-ferrierite catalysts acidity and cation siting to CH_4-NO_x-SCR activity. *Nuovo Cim.* **2008**, *123*, 1583–1595.
24. Çulfaz, A.; Yilmaz, A.K. Synthesis and characterization of ferrierite. *Cryst. Res. Technol.* **1985**, *20*, 11–19. [CrossRef]
25. Sannino, D.; Vaiano, V.; Ciambelli, P.; Murcia, J.; Hidalgo, M.; Navío, J.A. Gas-Phase photocatalytic partial oxidation of cyclohexane to cyclohexanol and cyclohexanone on Au/TiO_2 photocatalysts. *J. Adv. Oxid. Technol.* **2013**, *16*, 71–82. [CrossRef]
26. Vaiano, V.; Sannino, D.; Ciambelli, P. Sustainable gas phase selective photocatalytic oxidation of cyclohexane on $MoO_x/TiO_2/SiO_2$ catalysts. *Chem. Eng.* **2014**, *39*, 565–570.
27. Ciambelli, P.; Sannino, D.; Palma, V.; Vaiano, V.; Mazzei, R.S.; Eloy, P.; Gaigneaux, E.M. Photocatalytic cyclohexane oxidehydrogenation on sulphated MoO_x/γ-Al_2O_3 catalysts. *Catal. Today* **2009**, *141*, 367–373. [CrossRef]
28. Ciambelli, P.; Sannino, D.; Palma, V.; Vaiano, V. The effect of sulphate doping on nanosized and catalysts in cyclohexane photooxidative dehydrogenation. *Int. J. Photoenergy* **2008**, *2008*, 258631.
29. Ciambelli, P.; Sannino, D.; Palo, E.; Ruggiero, A. Improved stability of Co-ferrierite catalyst by Mn in dry–wet cycles of lean CH_4-SCR of NO_x. *Top. Catal.* **2007**, *42*, 177–181. [CrossRef]
30. Ciambelli, P.; Sannino, D.; Palma, V.; Vaiano, V. Photocatalysed selective oxidation of cyclohexane to benzene on MoO_x/TiO_2. *Catal. Today* **2005**, *99*, 143–149.

31. Einaga, H.; Futamura, S.; Ibusuki, T. Heterogeneous photocatalytic oxidation of benzene, toluene, cyclohexene and cyclohexane in humidified air: Comparison of decomposition behavior on photoirradiated TiO_2 catalyst. *Appl. Catal. B Environ.* **2002**, *38*, 215–225. [CrossRef]
32. ALOthman, Z.A. A review: Fundamental aspects of silicate mesoporous materials. *Materials* **2012**, *5*, 2874–2902. [CrossRef]
33. Ciambelli, P.; Corbo, P.; Gaudino, M.C.; Migliardini, F.; Sannino, D. Investigation of Co-based $DeNO_x$ catalysts for the treatment of natural gas lean-burn engine exhaust. *Top. Catal.* **2001**, *16-17*, 413–417. [CrossRef]
34. Pirone, R.; Ciambelli, P.; Moretti, G.; Russo, G. Nitric oxide decomposition over Cu-exchanged ZSM-5 with high SiAl ratio. *Appl. Catal. B: Environ.* **1996**, *8*, 197–207. [CrossRef]
35. Xu, Y.; Shu, Y.; Liu, S.; Huang, J.; Guo, X. Interaction between ammonium heptamolybdate and NH_4 ZSM-5 zeolite: The location of Mo species and the acidity of Mo/HZSM-5. *Catal. Lett.* **1995**, *35*, 233–243. [CrossRef]
36. Mejri, I.; Ayari, F.; Mhamdi, M.; Delahay, G.; Ksibi, Z.; Ghorbel, A. SCR of NO by NH_3 catalyzed by Mo-and V-exchanged zeolite: Effect of Mo precursor salt. *Microporous Mesoporous Mater.* **2016**, *220*, 239–246. [CrossRef]
37. Afanasiev, P.; Geantet, C.; Breysse, M.; Coudurier, G.; Vedrine, J.C. Influence of preparation method on the acidity of MoO_3 (WO_3)/ZrO_2 catalysts. *J. Chem. Soc. Faraday Trans.* **1994**, *90*, 193–202. [CrossRef]
38. Matralis, H.; Theret, S.; Bastians, P.; Ruwet, M.; Grange, P. Selective catalytic reduction of nitric oxide with ammonia using MoO_3/ TiO_2: Catalyst structure and activity. *Appl. Catal. B: Environ.* **1995**, *5*, 271–281. [CrossRef]
39. Lietti, L.; Alemany, J.; Forzatti, P.; Busca, G.; Ramis, G.; Giamello, E.; Bregani, F. Reactivity of V_2O_5- WO_3/TiO_2 catalysts in the selective catalytic reduction of nitric oxide by ammonia. *Catal. Today* **1996**, *29*, 143–148. [CrossRef]
40. Ng, K.Y.S.; Gulari, E. Molybdena on titania: I. Preparation and characterization by raman and fourier transform infrared spectroscopy. *J. Catal.* **1985**, *92*, 340–354. [CrossRef]
41. Quincy, R.B.; Houalla, M.; Proctor, A.; Hercules, D.M. Surface structure and thiophene hydrodesulfurization activity of molybdenum/titania catalysts. *J. Phys. Chem.* **1989**, *93*, 5882–5888. [CrossRef]
42. Tagiev, D.B.; Minachev, K.M. Catalytic properties of zeolites towards oxidation reactions. *Russ. Chem. Rev.* **1981**, *50*, 1009. [CrossRef]
43. Aliev, A.; Shabanova, Z.; Nadzhaf-Kuliev, U.; Medzhidova, S. Oxidative dehydrogenation of cyclohexane over modified zeolite catalysts. *Pet. Chem.* **2016**, *56*, 639–645. [CrossRef]
44. Sun, H.; Blatter, F.; Frei, H. Cyclohexanone from cyclohexane and O_2 in a zeolite under visible light with complete selectivity. *J. Am. Chem. Soc.* **1996**, *118*, 6873–6879. [CrossRef]
45. Palma, V.; Sannino, D.; Vaiano, V.; Ciambelli, P. Fluidized-Bed reactor for the intensification of gas-phase photocatalytic oxidative dehydrogenation of cyclohexane. *Ind. Eng. Chem. Res.* **2010**, *49*, 10279–10286. [CrossRef]
46. Ciambelli, P.; Sannino, D.; Palma, V.; Vaiano, V.; Bickley, R.I. Reaction mechanism of cyclohexane selective photo-oxidation to benzene on molybdena/titania catalysts. *Appl. Catal. A Gen.* **2008**, *349*, 140–147. [CrossRef]
47. Ciambelli, P.; Sannino, D.; Palma, V.; Vaiano, V.; Eloy, P.; Dury, F.; Gaigneaux, E.M. Tuning the selectivity of MoO_x supported catalysts for cyclohexane photo oxidehydrogenation. *Catal. Today* **2007**, *128*, 251–257. [CrossRef]
48. Maldotti, A.; Amadelli, R.; Vitali, I.; Borgatti, L.; Molinari, A. CH_2Cl_2-assisted functionalization of cycloalkenes by photoexcited $(n\mathrm{Bu}_4\mathrm{N})_4W_{10}O_{32}$ heterogenized on SiO_2. *J. Mol. Catal. A Chem.* **2003**, *204*, 703–711. [CrossRef]

© 2019 by the authors. Licensee MDPI, Basel, Switzerland. This article is an open access article distributed under the terms and conditions of the Creative Commons Attribution (CC BY) license (http://creativecommons.org/licenses/by/4.0/).